

μFLU08-226

NUMERICAL SIMULATION OF SINGLE ARTIFICIAL CILIUM MAGNETIC DRIVEN MOTION IN A SEMI-INFINITE DOMAIN

Dragos Isvoranu¹

Dept. of Thermodynamics, University Politehnica of Bucharest, 313, Spl. Independentei, Sect. 6, Bucharest
060042, Romania
ddisvoranu@gmail.com

Daniel Ioan, Petrisor Parvu

Fac. of Electrical Engineering, University Politehnica of Bucharest, 313, Spl. Independentei, Sect. 6,
Bucharest 060042, Romania; Fac. of Aerospace Engineering, University Politehnica of Bucharest, 1, Polizu,
Bucharest 060012, Romania
daniel@lmn.pub.ro, parvu@aero.pub.ro

KEY WORDS

micro-fluidics, magnetic-fluid-structure interaction

ABSTRACT

The current paper deals with a completely novel method of fluid manipulation technology in micro-fluidics systems, inspired by nature, namely by the mechanisms found in ciliates. More information on this subject can be found at <http://www.hitech-projects.com/euprojects/artic/>. In order to simulate the drag forces acting on the artificial cilium, we have developed a computer code that is based on fundamental solutions of Stokes flow in a semi-infinite domain. The actuation mechanism consists of a bi-directional rotating excitation magnetic field. Two situations have been considered: hard-magnetic material and soft-magnetic for the cilium. In the first case, it was considered that the cilium is uniformly magnetized and immersed in a uniform magnetic field of magnetic density B , such that the magnetic torque on every element of the cilium depends mainly only on the relative position between the element and the constant direction of vector B . In the second case, the magnetization induced by the magnetic field was calculated in a separate routine based on the Integral Nonlinear Equations Approach with 1D discretization of wire (cilium). Distal-end mass flows are computed for several cilium configurations resulting non-zero average mass flow rates. The outcome and originality of this paper consist on assessing magnetic actuation as a practical tool for obtaining a consistent one-directional fluid flow.

1. INTRODUCTION

Cilia are thin hair-like cell appendices responsible for many essential biological functions. They have been the subject of numerous research studies in biology and medicine for some 250 years. Theoretical research in

¹ Corresponding author

this domain has mainly been oriented towards understanding the biochemical engine driving such complex movements and providing valuable insights of the interaction between the deformations of the elastic structure and the viscous incompressible fluid surrounding it. Based on their typical dimensions and physical properties of biological fluids we are able to assess that the Reynolds number of such flows is of the order of unity or less. In this case not only the flow is laminar but it is dominated by viscous forces that makes it close to a classical Stokes flow. On the other hand, the dynamics of such elastic structure lacks the inertial term because of the very small characteristic mass.

The on-going miniaturization in a variety of scientific domains especially biochemistry and medicine requires manipulation of smaller and smaller volumes of biological fluids such as blood, saliva, urine, or polymer solutions. Examples of such applications are micro-channel cooling for electronics, inkjet printing for displays and biomedical applications, controlled drug delivery systems and biosensors. Also, the nature of the manipulation may be quite broad: transportation, mixing, sorting, deforming, or rupturing.

One of the most interesting and useful cilia functionalities is propulsion, meaning either self-propulsion of the organism or inducing fluid flow around a stationary organism at micron-scale dimensions.

The movement of the individual cilia is asymmetric, i.e. a deformation cycle consists of an effective stroke and a recovery stroke. During the effective stroke the cilium behaves like a rigid rod while in the recovery stroke it bends and rolls back to the original position so that a resultant fluid transport in one direction is induced. Also, the cilia operate collectively by having a slight phase lag between their movements, so that a meta-chronic wave is created.

Our main objective is to assess the feasibility of a controlled magnetic actuation for a cilium placed into micro-fluidic semi-infinite channel. The actuation mechanism consists of a bi-directional rotating excitation magnetic field that interacts with the magnetized cilium. Velocity fields and distal-end mass flows are computed for several cilium configurations (perpendicular or near-tangential at substrate).

2. PHYSICAL MODEL

The cilium is modeled as an inextensible cylindrical filament of length L and circular cross section of radius a . The slenderness of the cilium is defined by ratio $\varepsilon = a/L \ll 1$. The center line of the filament is parameterized by its arc-length s ($0 \leq s \leq L$). The null value corresponds to the anchor point where the cilium is attached to the substrate surface; $s=L$ at the distal end. Two coordinate systems (CS) are defined, one fixed at the anchor and a Lagrangean one attached to an arbitrary point on the cilium. Due to the axial symmetry in the magnetic field density we shall restrict our analysis to planar case. Hence, the coordinate systems are (x,y) , global, and (T,N) , local, as illustrated in figure 1. The angle between the tangential direction in local CS and the x axis in global CS is denoted α , being a function of arc-length and time $\alpha = \alpha(s,t)$.

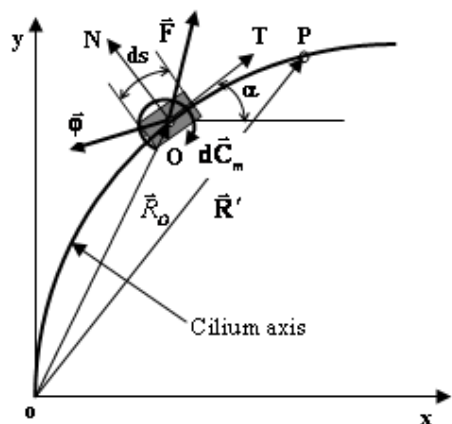


Figure 1: Geometry and forces.

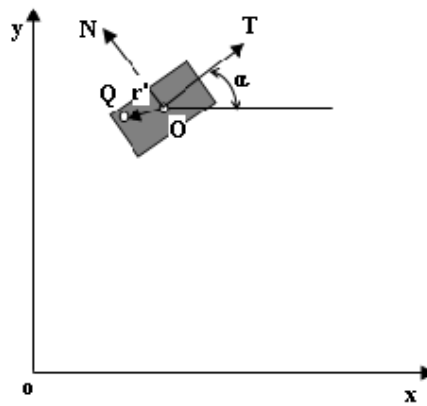


Figure 2: Local and global coordinate systems

The parameterized equations of the center line points are given by

$$x(s,t) = \int_0^s \cos(\xi,t) d\xi, \quad y(s,t) = \int_0^s \sin(\xi,t) d\xi \quad (1)$$

The driving engine is represented by the magnetic torque $\mathbf{C} = \mathbf{C}(s,t)$. The response from the elastic structure is denoted by the shear force $\mathbf{F} = \mathbf{F}(s,t)$ and $\boldsymbol{\varphi} = \boldsymbol{\varphi}(s,t)$ are the viscous forces per unit length (drag forces) exerted by the surrounding fluid. Here and in the following the bold typeface denotes vector quantities. The velocity of the current cross section s is denoted by $\mathbf{V} = \mathbf{V}(s,t)$.

From the mechanical point of view, we consider that cilium is in mechanical equilibrium at every moment of time.

2.1. Equations of motion

Considering a finite volume of the cilium along the arc-length ds the balance of forces and moments in the local Frenet coordinate system reads:

$$\boldsymbol{\varphi}_N = F_{N,s} + F_T \boldsymbol{\alpha}_s \quad (2)$$

$$\boldsymbol{\varphi}_T = F_{T,s} - F_N \boldsymbol{\alpha}_s \quad (3)$$

$$C_{m,s} + F_N = EI \boldsymbol{\alpha}_{ss} \quad (4)$$

where subscripts N , T means normal and tangential components and s , t denote arc-length and time derivation. $C_{m,s}$ is the derivative of the magnetic torque. The drag force components are specified through linear dependence on velocity components

$$\boldsymbol{\varphi}_N = -C_N V_N + \mathbf{g}_N \quad \boldsymbol{\varphi}_T = -C_T V_T + \mathbf{g}_T \quad (5)$$

$$\mathbf{g}_N = C_N \mathbf{G}_N \quad \mathbf{g}_T = C_T \mathbf{G}_T \quad (6)$$

where G_N and G_T are the local CS components of the velocity induced at current location by the flow field generated by superposition of Stokes equation fundamental solutions and their image systems [2]. The normal and tangential specific drag coefficients are denoted by C_N and C_T . Time differentiation of geometrical relations (1) leads to kinematic conditions:

$$V_{N,s} = \boldsymbol{\alpha}_t - V_T \boldsymbol{\alpha}_s \quad (7)$$

$$V_{T,s} = V_N \boldsymbol{\alpha}_s \quad (8)$$

2.2. Flow equations

Taking into account that viscous forces prevail in this type of flow, the movement of the fluid can be modeled by superposition of the fundamental solutions of Stokes equations

$$\nabla p = \mu \Delta \mathbf{U} + \mathbf{f}, \quad \nabla \cdot \mathbf{U} = 0 \quad (9)$$

$$\mathbf{f} = \boldsymbol{\varphi} \delta(\mathbf{R}' - \mathbf{R}_O) \quad (10)$$

where p is pressure per unit length, μ the dynamic viscosity of the fluid, \mathbf{U} velocity vector per unit length, $\boldsymbol{\varphi}$ the drag force per unit length acting at the point defined by position vector \mathbf{R}_O [1]. In the local cartesian coordinates the velocity \mathbf{V} of the cross section s_0 , $q < s_0 < L - q$, reads

$$\mathbf{V}(s_0,t) = -\frac{1}{C_T} \boldsymbol{\varphi}_T(s_0,t) \mathbf{t} - \frac{1}{C_N} \boldsymbol{\varphi}_N(s_0,t) \mathbf{n} + \mathbf{G}(s_0,t) \quad (11)$$

$$\begin{aligned} \mathbf{G}(s_0,t) = & \int_{|s-s_0|>q} \mathbf{U}_s(\mathbf{R}_O(s_0,t), \mathbf{R}'(s,t), -\boldsymbol{\varphi}(s,t)) ds + \\ & + \int_{0 \leq s \leq L} [\mathbf{V}_{st}(\mathbf{R}_O(s_0,t), \mathbf{R}'(s,t), -\boldsymbol{\varphi}(s,t)) + \mathbf{V}_{di}(\mathbf{R}_O(s_0,t), \mathbf{R}'(s,t), -a^2 \boldsymbol{\varphi}(s,t)/4\mu)] ds \end{aligned} \quad (12)$$

The drag coefficients

$$C_T = \frac{8\pi\mu}{-2 + 4\ln(2q/a)} \quad C_N = \frac{8\pi\mu}{1 + 2\ln(2q/a)} \quad (13)$$

are obtain after integrating the tangential velocity induced by the Stokeslets over a cuasi-cylindrical domain $[s_0 - q, s_0 + q]$ with an error of $O(a/q^2)$ [2].

2.3. Magnetostatic equations

The magnetic actuation is produced by a rotating magnetic field generated with either longitudinal or longitudinal and transversal coils. Harmonic excitation of coils is assumed. Taking into account the negligible lateral dimension of the cilium, we infer z-axis symmetry of the magnetic field. Two cases are of interest: permanently magnetic material with saturation magnetization (PMM) and super paramagnetic material without hysteretic behaviour (SPM). In the first case, the magnetic torque per control volume for a constant longitudinal saturation magnetization in the local CS is simply

$$dC_m = M_{sat} \pi a^2 [B_x \sin \alpha(s,t) - B_y \cos \alpha(s,t)] ds \quad (14)$$

In the second case the magnetization induced by an external magnetic field \mathbf{H}_0 in an arbitrary point P for a geometry presented in figure 1 has the expression [5]

$$\mathbf{M}(\mathbf{R}') + \frac{\chi}{4\pi} \int_{\Omega_m} \nabla \cdot \mathbf{M}(\mathbf{R}) \nabla \left[\frac{1}{|\mathbf{R}' - \mathbf{R}|} \right] dV = \chi \mathbf{H}_0(\mathbf{R}') \quad (15)$$

where Ω_m is the wire-flap volume, \mathbf{M} magnetization and χ magnetic susceptibility. In order to evaluate the integral in (15) it is convenient to discretize the wire into N smaller control volumes Ω_i of length $2l$ over which the magnetization divergence can be approximated by the finite difference

$$\nabla \cdot \mathbf{M} \cong \frac{M_T^{i+1} - M_T^i}{2l} \quad (16)$$

where superscripts $i, i+1$ denote the consecutive discretization points of the cilium center line. Hence, (15) becomes

$$\mathbf{M}(\mathbf{R}') + \frac{\chi}{4\pi} \sum_{i=1}^N \frac{M_T^{i+1} - M_T^i}{2l} \int_{\Omega_i} \nabla \left[\frac{1}{|\mathbf{R}' - \mathbf{R}'|} \right] dV^i = \chi \mathbf{H}_0(\mathbf{R}') \quad (17)$$

The remaining integral in (17) has analytic solution for flap configuration [4]. In the case of slender cylindrical cilium, analytic solution of the respective integral can be inferred if we can neglect its dependence on the azimuthal angle such that the local CS becomes axial-symmetric. The position vector \mathbf{R} of a current point Q (x', y') in local CS (see figure 2) reads

$$\mathbf{R} = \mathbf{R}_o + \mathbf{r}' = \left(\frac{x^i + x^{i+1}}{2} + x, \frac{y^i + y^{i+1}}{2} + y \right) \quad (18)$$

$$x = x' \cos \alpha^{i+1/2} - y' \sin \alpha^{i+1/2} \quad (19)$$

$$y = x' \sin \alpha^{i+1/2} + y' \cos \alpha^{i+1/2}$$

where $\alpha^{i+1/2} = 0.5(\alpha^i + \alpha^{i+1})$ is the angle between tangent and horizontal at the center of element Ω_i . The coordinates of the calculation point P are given by

$$\mathbf{R}' = (x^j, y^j) \quad (20)$$

The element volume reads $dV^i = 2\pi y' dy' dx'$. With these notations the integral in (17) becomes

$$\begin{aligned}
 & \int_{\Omega_i} \nabla \left(\frac{1}{|\mathbf{R} - \mathbf{R}'|} \right) 2\pi y' dx' dy' = \\
 & = 2\pi \int_{-l}^l \int_0^a \left[\frac{\partial}{\partial x'} \left(\frac{1}{|\mathbf{R} - \mathbf{R}'|} \right) \mathbf{t}^{i+1/2} + \frac{\partial}{\partial y'} \left(\frac{y'}{|\mathbf{R} - \mathbf{R}'|} \right) \mathbf{n}^{i+1/2} - \frac{\mathbf{n}^{i+1/2}}{y' |\mathbf{R} - \mathbf{R}'|} \right] y' dx' dy' = \quad (21) \\
 & = 2\pi \left[I_1^{j,i+1/2} \mathbf{t}^{i+1/2} + (I_2^{j,i+1/2} - I_3) \mathbf{n}^{i+1/2} \right]
 \end{aligned}$$

Basic calculus allows determining analytic solutions for the coefficients of influence I_1 , I_2 and I_3 , such that equation (17) is re-written as

$$\mathbf{M}(\mathbf{R}') + \frac{\chi}{2} \sum_{i=1}^N \left[\frac{M_T^{i+1} - M_T^i}{2l} \right] \left[I_1^{j,i+1/2} \mathbf{t}^{i+1/2} + (I_2^{j,i+1/2} - I_3) \mathbf{n}^{i+1/2} \right] = \chi \mathbf{H}_0(\mathbf{R}') \quad (22)$$

Once the magnetization vector $\mathbf{M}(\mathbf{R}')$ is known we are able to determine the self field strength generated by this magnetization by simply neglecting the external field in eq.(17)

$$\mathbf{H}_{self}(\mathbf{R}') = -\frac{1}{2} \sum_{i=1}^N \frac{M_T^{i+1} - M_T^i}{2l} \int_{\Omega_i} \nabla \left[\frac{1}{|\mathbf{R}' - \mathbf{R}|} \right] dV^i \quad (23)$$

Using (21) we finally get

$$\mathbf{H}_{self}(\mathbf{R}') = -\frac{1}{2} \sum_{i=1}^N \left[\frac{M_T^{i+1} - M_T^i}{2l} \right] \left[I_1^{j,i+1/2} \mathbf{t}^{i+1/2} + (I_2^{j,i+1/2} - I_3) \mathbf{n}^{i+1/2} \right] \quad (24)$$

Based on the constitutive relation we obtain the self field density

$$\mathbf{B}_{self} = \mu_0 \mu_r \mathbf{H}_{self} \quad (25)$$

where μ_0, μ_r represents the magnetic permeability of the vacuum and the relative permeability of the super paramagnetic material (SPM). Hence, the magnetic torque reads

$$d\mathbf{C}_m^{i+1/2} = \mathbf{M}^{i+1/2} \times (\mathbf{B}_0^{i+1/2} + \mathbf{B}_{self}^{i+1/2}) dV^i \quad (26)$$

The susceptibility χ of the SPM is defined as $\chi = \mu_r - 1$. Numerical derivation of the magnetic torque has been used in order to ensure normal equilibrium condition (4).

2.4. Magnetic actuation

In both cases of interest, the rotating magnetic field $\mathbf{B}_0 = (B_x, B_y)$ is modeled by the following time dependence

$$\begin{aligned}
 B_x(t) &= B \sin(2\pi ft) \\
 B_y(t) &= B \sin\left(2\pi ft + \frac{\pi}{12}\right)
 \end{aligned} \quad (27)$$

where f is frequency.

3. NUMERICAL APPROACH

The derivative of magnetic torque used in the equilibrium condition (4) provides the active force denoted by

$$S = \frac{dC_m}{ds} \quad (28)$$

Starting from relations (2)-(8) and (11)-(12) a proper non-dimensionalization was performed

$$\bar{S} = \frac{S}{S_0}, \quad \bar{F} = \frac{F}{S_0}, \quad \bar{s} = \frac{s}{L}, \quad \bar{g} = \frac{gL}{S_0}, \quad \bar{\phi} = \frac{\phi L}{S_0}, \quad \bar{t} = \frac{t}{T} = ft \quad (29)$$

$$C_{TN} = \frac{C_T}{C_N}, \quad C_{NT} = \frac{C_N}{C_T}, \quad \bar{C}_N = \frac{C_N L^2 f_0}{S_0} \quad (30)$$

where S_0 is a characteristic value of the active force module.

The following system of equations describes the fluid structure interaction [3].

$$\bar{F}_N = \frac{EI}{S_0 L^2} \alpha_{ss} + \bar{S} \quad (31)$$

$$\bar{F}_{T_{ss}} = (1 + C_{TN}) \bar{F}_{N_s} \alpha_s + C_{TN} \bar{F}_T \alpha_s^2 + \bar{F}_N \alpha_{ss} - C_{TN} \bar{g}_N \alpha_s + \bar{g}_{T_s} \quad (32)$$

$$\bar{C}_N \alpha_t = C_{NT} (\bar{F}_N \alpha_s^2 - \bar{F}_{T_s} \alpha_s + \bar{g}_T \alpha_s) - (\bar{F}_{N_{ss}} + \bar{F}_T \alpha_{ss} + \bar{F}_{T_s} \alpha_s) + \bar{g}_{N_s} \quad (33)$$

where E is the elastic modulus of the wire and I is the inertia momentum of its circular section. The boundary conditions are given by

$$\alpha_s(0, t) = 0, \quad \alpha_s(L, t) = 0 \quad (34)$$

$$\alpha_{sss}(0, t) = -\frac{S_0 L^2}{EI} \bar{S}_s(0, t); \quad \alpha_{ss}(L, t) = -\frac{S_0 L^2}{EI} \bar{S}(L, t) \quad (35)$$

$$\bar{F}_{N_s}(0, t) = \bar{F}_{T_s}(0, t) = 0; \quad \bar{F}_N(L, t) = \bar{F}_T(L, t) = 0 \quad (36)$$

The initial condition in both cases reads

$$\alpha(s, 0) = \begin{cases} \pi/18 & s = 0 \\ (\pi/2 + \phi - \pi/18) \left(s \frac{N}{L} - 1 \right) \\ \pi/18 + \frac{(\pi/2 + \phi - \pi/18) \left(s \frac{N}{L} - 1 \right)}{(N-1)} & s \in \left[\frac{L}{N}, L \right] \end{cases} \quad (37)$$

where ϕ is a variable angle that defines the bending of the distal end of the wire. Based on an adequate linear discretization of the arc-length of the wire (31 segments, for example) and using a Crank-Nicholson finite difference scheme, the system (31)-(37) is solved for the time-depending parameterization of the wire $\alpha = \alpha(s, t)$.

Basic algebra enables us to transform the quite cumbersome system (22) into a simpler linear system for which Gaussian elimination can be directly applied.

$$M_T^j + \frac{\chi}{2} \sum_{i=1}^N \left[\frac{M_T^{i+1} - M_T^i}{2l} \right] \left[I_1^{j,i+1/2} \cos(\alpha^j - \alpha^{i+1/2}) + (I_2^{j,i+1/2} - I_3) \sin(\alpha^j - \alpha^{i+1/2}) \right] = \chi H_{0,T}^j \quad (38)$$

The same stands also for the determination of the self field strength.

$$H_{self,T}^j = -\frac{1}{2} \sum_{i=1}^N \left[\frac{M_T^{i+1} - M_T^i}{2l} \right] \left[I_1^{j,i+1/2} \cos(\alpha^j - \alpha^{i+1/2}) + (I_2^{j,i+1/2} - I_3) \sin(\alpha^j - \alpha^{i+1/2}) \right] \quad (39)$$

The fluid domain surrounding the cilium, depicted in Figure 3, is discretized using a rectangular grid. The velocity field in this domain is calculated based on the singular solution of Stokes equation (Stokeslet) for all nodes of the grid (x_g, y_g) .

$$\mathbf{V}(x_g, y_g, t) = \int_{0 \leq s \leq L} \mathbf{U}_s(\mathbf{R}(x_g, y_g), \mathbf{R}'(s, t), -\phi(s, t)) ds \quad (40)$$

Using this velocity field we are able to determine the x-coordinate mass flow rate generated by the magnetic actuation of the cilium in every section $x = ct$ of the domain.

$$\dot{m}_x = L \rho_w \int_{y=0}^{y=1.4} v_x dy \quad (41)$$

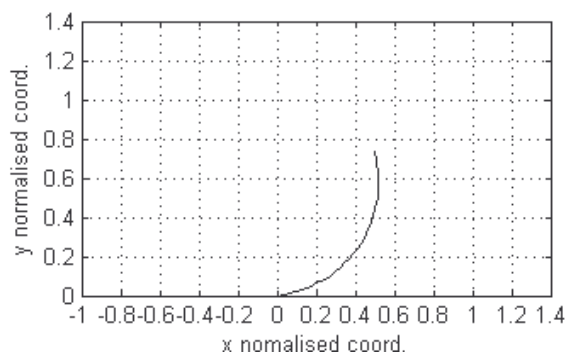


Figure 3. Discretization of the analysis domain

where ρ_w is the density of water.

4. RESULTS

A computer code has been devised in order to perform the necessary simulations. All external inputs and other parameters range of variation have been imposed such that to ensure mechanical and geometrical stability. The simulations had two purposes. The first goal was to demonstrate the feasibility of artificial cilium actuation based on bi-directional rotating magnetic field. Pictures of cilium position and velocity field at every other quarter period are presented in Figures 4 and 5 for SPM and PMM materials illustrating several salient features. The most important is the consistent difference between the amplitudes of the cilium movement in the two cases (Figure 6). Although in both cases we used the same external parameters presented in Table 1 and initial conditions, $\phi = \pi/12$, only in the PMM case, the wire movement has the same intrinsic period (T) as the one of the external field. In the SPM case, we observe that the superposition of the self field and the exterior field produces a cyclic movement with half the period of the external field, denoted T^* (Figure 7). At first glance the velocity field in both cases looks alike, although the top velocity values and geometrical extend are somehow higher in PMM case.

A more subtle introspection into the fluid velocity field is performed by evaluating the mass flow rate and under these auspices we turn our attention to the other goal of our analysis. In our opinion the most relevant quantity measuring the performance of fluid manipulation based on artificial cilium actuation is mass flow rate. Henceforth, we embark upon a comparison of mass flow rates in several configurations.

Parameter	L	A	q	F	μ	E	$B_x=B_y$	ρ_w	μ_0	M_{sat}
Value	100	1	10	25	0.001	10^6	0.01	1000	$4\pi \cdot 10^{-7}$	20
Unit	μm	μm	μm	Hz	Ns/m^2	Pa	T	kg/m^3	H/m	kA/m

Table 1.

The instantaneous values of the mass flow rate in the left and right boundaries of analysis domain presented in Figure 7 seem to advocate for the superiority of the PMM case. The x-coordinate distribution of the time averaged values are more relevant for the efficiency of the device. Figure 8 shows that, for the same bending angle ϕ , the time averaged x-coordinate mass flow rate distribution is by far superior in the SPM case than PMM case (Figure 9). Although the area of the SPM cycle is much smaller than that of PMM cycle ($\sim 1/50$), the outcome (time averaged mass flow rate) is much larger in the first case. Obviously, having a sustainable mass flow in certain direction is linked to the necessity of ensuring an asymmetric movement along the perpendicular direction to the flow. From this point of view, the degree of asymmetry in the PMM case is

much lower than in the SPM case, as can easily be seen from Figures 6 and 7. We conclude that the intrinsic value of the area the distal end of the flaps or cilium circumvents is of little relevance in comparing artificial micro-flow devices performances. The pertinent quantity suiting this purpose remains the time averaged mass flow rate. From the geometrical point of view it seems that for the curled cilium an important parameter is the distal end bending angle which we have varied in the range $0 \div \pi/12$. Larger values would have led to loosing mechanical and geometrical stability. As can easily be seen in Figures 8 and 9, the most efficient configuration is for $\phi = \pi/12$. In the SPM case, an insight of the relative magnitude of the self induction field for relative permeability $\mu_r = 5.4$ and $\phi = \pi/12$ has been presented in Figure 10. Another interesting feature of this type of material is that illustrated in Figure 11. The higher the relative permeability is over $\mu_r = 9$ the lower mass flow rate the device produces. At the same time, the direction of the flow is reversed. The same applies in the case the relative permeability is in the range $[3.5, 5.4]$ except flow reversal. Between 5.4 and 9 and below 3.5 cilium loses mechanical and geometrical stability for the 10 mT external excitation induction.

5. CONCLUSIONS AND ACKNOWLEDGEMENTS

The paper has dealt with a most complex engineering problem encompassing three domains of physics, magnetism, mechanics and fluid flow. We have proven the feasibility of magnetic actuation of the cilium through rotating bi-directional field. Several external and internal parameters have been varied in order to catch the salient features of the micro-fluidic device behavior. Consequently, it is apparent that for a circular wire geometry and a 10 mT external excitation the solution providing the highest mass flow rate implies using a super paramagnetic material with relative permeability of 5.4 and distal end bending angle of $\pi/12$. Further work needs to be done for 3D geometries like flap and flap clusters.

ACKNOWLEDGEMENTS

This work has been supported through grant ARTIC FP6-2004-NMP-TI4.

REFERENCES AND CITATIONS

- [1] Chwang, A. T., & Yao-Tsu Wu, T. (1974). Hydromechanics of low-Reynolds-number flow. Part2. Singularity method for Stokes flows. *J. Fluid Mech.*, **67**, part 4, 787-815.
- [2] Gueron, S., & Liron, N. (1992). Ciliary motion modeling and dynamic multicilia interactions. *Biophys. J.*, **63**, 1045-1058.
- [3] Gueron, S., & Levit-Gurevich, K. (1998). Computation of the internal forces in cilia: Application to ciliary motion, the effects of viscosity and interactions. *Biophys. J.*, **74**, 1658-1676.
- [4] Ioan, D., & Hantila, I. F., Rebican, M., Constantin, C. (1998). FLUXSET sensor analysis based on nonlinear magnetic wire of the core. In *Electromagnetic Nondestructive Evaluation (II)*, 160-169. IOS Press, Amsterdam.
- [5] Jackson, J.D. (1974). *Classical Electrodynamics*. John Wiley & Sons.

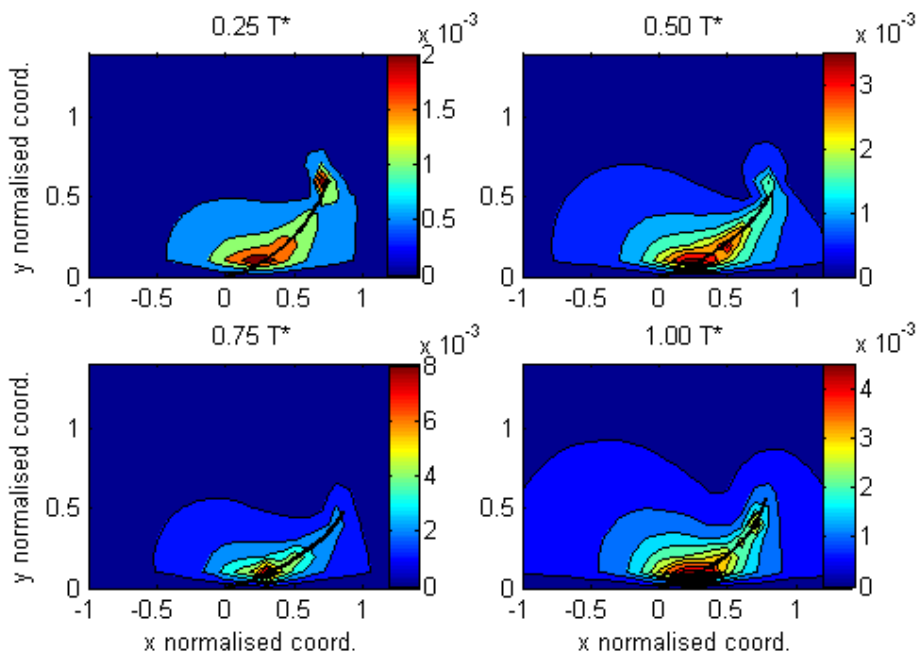


Figure 4. SPM velocity field and cilium position. $\mu_r = 5.4$, $\phi = \pi/12$

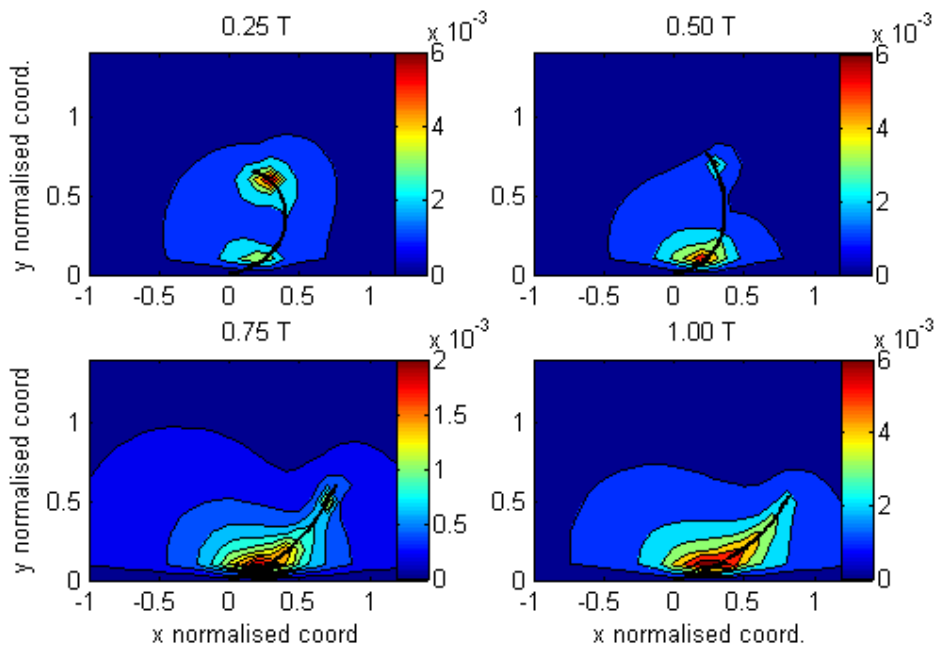


Figure 5. PPM velocity field and cilium position. $\phi = \pi/12$

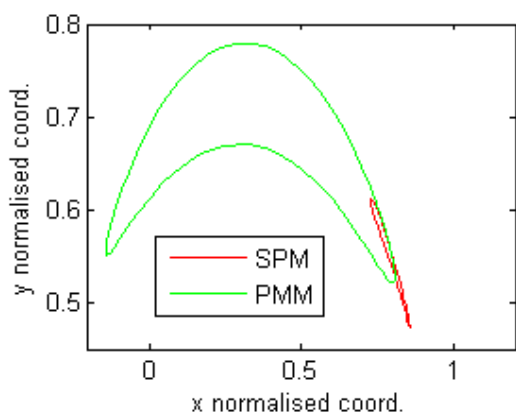


Figure 6. Distal end orbits $\mu_r = 5.4, \phi = \pi/12$.

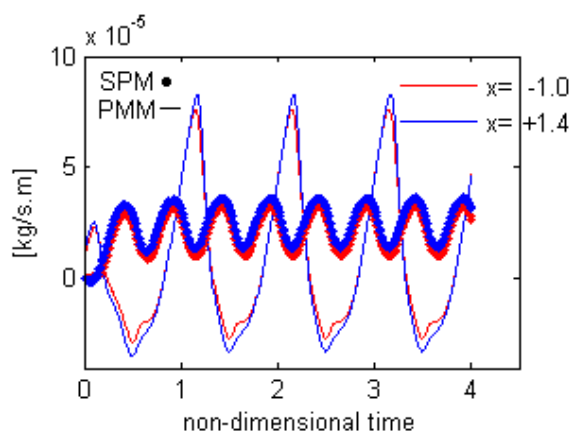


Figure 7. Instantaneous mass flow rate at left and right boundaries $\mu_r = 5.4, \phi = \pi/12$.

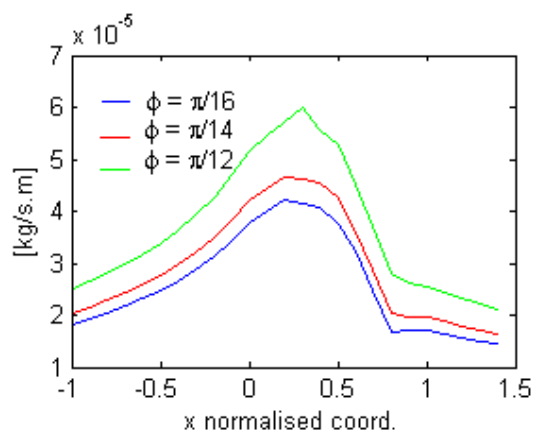


Figure 8. Time averaged mass flow rate for the SPM case. $\mu_r = 5.4$.

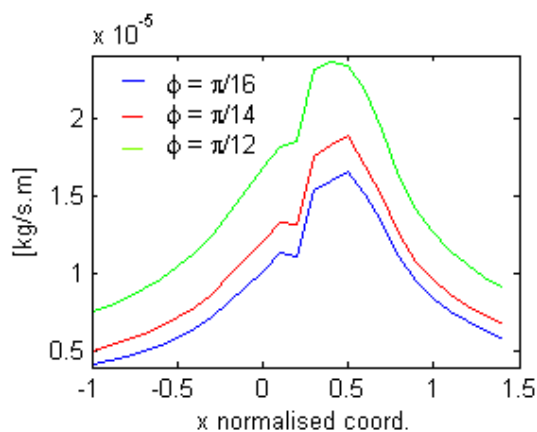


Figure 9. Time averaged mass flow rate for the PPM case

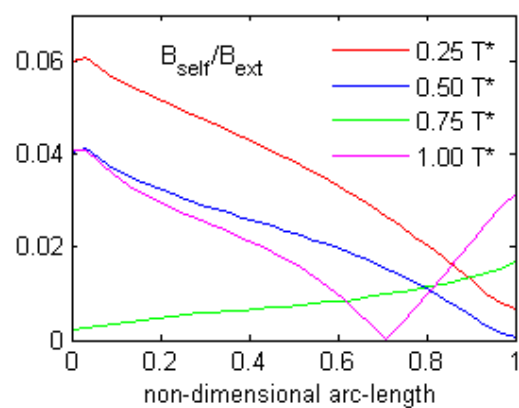


Figure 10. Relative magnitude of the self induction field. $\mu_r = 5.4, \phi = \pi/12$.

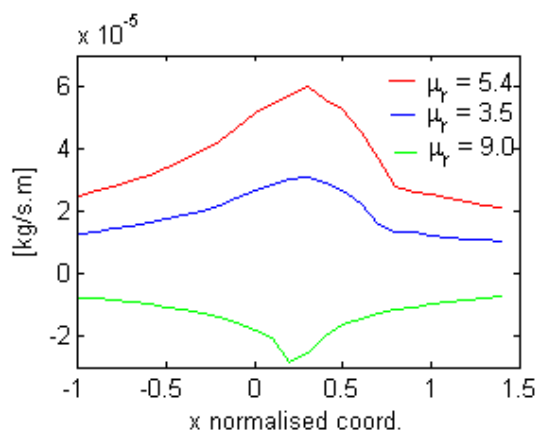


Figure 11. Time averaged mass flow rate for the SPM case $\phi = \pi/12$.